Experimental Investigation of Transient Critical Heat Flux of Water-Based Zinc-Oxide Nanofluids

Vivek I. Sharma[a,1], Jacopo Buongiorno[a,2], Thomas J. McKrell[a], L.W. Hu[b]

[a] Department of Nuclear Science and Engineering, Massachusetts Institute of Technology, 77 Massachusetts Avenue, Cambridge, MA-02139, USA

vivekis@mit.edu, jacopo@mit.edu, tmckrell@mit.edu

[b] Nuclear Reactor Laboratory, 138 Albany Street, Massachusetts Institute of Technology, Cambridge, MA-02139, USA

lwhu@mit.edu

Abstract

Pool boiling experiments were conducted for sandblasted stainless steel (grade 316) plate heaters submerged in deionized (DI) water and water-based zinc-oxide nanofluid, for transient heat flux conditions with power through the heaters increasing quadratically with time. Heat flux in the experiments was increased from zero to CHF in short time frames of 1, 10 and 100 s. Consistent with previous studies, transient CHF for DI water was higher than steady state CHF, and CHF increased with decreasing duration of the transient. Additionally, it was observed that for nanofluid tests, a porous and hydrophilic nanoparticle layer started to deposit on the heater surface in short time frames of 10 and 100 s, and this layer was responsible for the enhanced CHF compared to DI water. However, for the 1 s tests, nanoparticle deposition did not occur and consequently the CHF was not enhanced. Finally, experiments with heaters pre-coated with nanoparticles were performed and it was found that CHF was enhanced for all transient durations down to 1 s, establishing firmly that the CHF enhancement occurs due to surface modifications by the deposited nanoparticles, and not by nanoparticles suspended in solution.

Keywords

Transient CHF; departure from nucleate boiling; boiling crisis; pool boiling

Nomenclature

α	temperature coefficient of resistivity [Ω/Ω-^{0}C]
A_{ht}	area of heat transfer [m^2]
CHF	critical heat flux [kW/m^2]
c_p	specific heat capacity [J/kg-^{0}C]
DAS	data acquisition system

[1] Present Address: 2501 NW 229th Ave, RA3-355/458, Hillsboro, OR – 97124, USA
[2] Corresponding author. Email: jacopo@mit.edu, Ph: +1-617-253-7316, Fax: +1-617-258-8863

HTC	heat transfer coefficient [kW/m^2-^0C]
I	current [A]
PBF	pool boiling facility
q''	heat flux [kW/m^2]
ρ	density [kg/m^3]
R	resistance [Ω]
R_{100}	resistance at 100 ^0C [Ω]
R_a	average surface roughness [μm]
t_0	ramp time for current for transient tests [s]
T_{bulk}	bulk heater temperature [^0C]
ΔV	potential drop across heater [V]

1. Introduction

Nucleate boiling is a very efficient mode of heat transfer owing to the large energy required to realize the phase change from liquid to vapor. Therefore, several important industrial applications utilize nucleate boiling to remove large heat fluxes from hot surfaces. These include nuclear reactors, miniature electronic devices, refrigeration and cryogenic systems, chemical and thermal reactors, among others. However, it is well known that there exists a critical value of the heat flux at which the heat transfer mechanism changes from the highly efficient nucleate boiling to extremely inefficient film boiling. This limiting heat flux is called Critical Heat Flux (CHF). The deterioration in the process of heat removal from the hot surface, due to the initiation of film boiling, can cause rapid excursions in the temperature of the heat source which can lead to destruction of the boiling surface. Therefore, in most applications of boiling, the system is required to operate at power levels below that corresponding to CHF. As such, there is considerable interest in increasing CHF since, everything else being constant, a higher value of CHF allows for higher power density in thermal systems, which in turn makes these systems more compact and ultimately more economic. One way to increase CHF is to suspend a small amount of nanoparticles in the base fluid to form a suspension called nanofluid [1, 2]. The main objective of this paper is to report on an experimental study that examined the effect of nanofluids on CHF behavior for rapidly increasing heat flux excursions, with excursion times less than 100 s. The structure of the paper is as follows: Section 3 reviews the literature on nanofluids and transient CHF; Section 3 describes the preparation and characterization of the nanofluids used in the experiments; the experimental procedure is described in Section 4. The results are summarized in Section 5, followed by the discussion in Section 6 and conclusions in Section 7.

2. Literature Review

2.1 Nanofluids

Several techniques to enhance the CHF have been explored. According to Rohsenow et al [3] they can be classified into *active* (requiring external changes to the heater) or *passive* (requiring no external changes to the heater) methods. Typical active approaches include vibration of the heated surface or the cooling fluid (to increase the bubble departure frequency), heater rotation (to promote bubble departure from and liquid deposition onto the heater surface) and applying an external electric field (to facilitate the bubble departure from the surface by dielectrophoretic force), and passive approaches include coating the surface with porous coatings (to increase the number of active nucleation sites) and oxidation or selective fouling of heater surface (to increase surface hydrophilicity) [4]. A recent passive approach that has garnered increased attention worldwide is to create a colloidal suspension of solid nanoparticles in water or other base fluid, called nanofluids [1, 2]. There are various materials of choice for the dispersed nanoparticles – chemically stable metals (such as Cu, Au and Ag), metal oxides (such as Al_2O_3, SiO_2 and ZrO_2) and different forms of carbon (such as diamond, graphite and fullerene). Boiling tests have shown these engineered nanofluid coolants to have a significantly higher CHF (generally, an enhancement ranging from 20% to more than 100%) compared to water. You et al were the first researchers to observe a considerable CHF enhancement in alumina nanofluids [5]. Since then, nanofluid boiling has generated a lot of curiosity and efforts to understand the underlying CHF enhancement mechanism. Researchers also investigated changes of the heat transfer coefficient (HTC) for nanofluids compared to water. The findings from the literature can be summarized as follows:

- All researchers observed deposition of a layer of nanoparticles on the boiling surface during the course of nanofluids boiling. According to common consensus by researchers [7-12], this nanoparticle deposition layer is the primary mechanism for CHF enhancement, as it changes the porosity and the hydrophilicity of the surface, altering the dynamics of the three phase interface at the heater surface.
- Most of the studies report significant CHF enhancement (up to 200%) with nanofluids compared to water [5-18].
- Even relatively low concentrations (<1% by volume) of nanoparticles are capable to enhance CHF.
- Researchers have reported contradicting findings on the effect of nanofluid on HTC. While some studies have shown an enhancement in HTC for nanofluids compared to water [12, 13, 19-21], others show deterioration [7, 14, 22-24] and few document no effect of suspended nanoparticles on HTC [5, 6, 8, 10, 11].

2.2 Transient CHF

It is well documented that the value of the transient CHF can be significantly different from the steady state CHF value [25-33]. Most of the studies reported are for an exponentially increasing volumetric power input given by $Q = Q_o e^{t/\tau}$, where Q_o is the initial power level per unit volume in the heater and τ is the time constant for the transient. There have been several attempts to understand the mechanism for transitions from conduction, natural convection and nucleate boiling regimes to film boiling regime, due to exponentially increasing heat inputs with various fluids, such as water, and highly wetting fluids such as liquid nitrogen, liquid helium and ethanol [25-33]. Sakurai and Shiotsu, first, suggested that the boiling curve for transient tests is slightly different from that of steady heat flux tests [26, 27]. Sakurai et al also observed that for a fixed

heat flux value, HTC for transient tests after boiling initiation was lower than that for steady state tests [29]. This was explained as follows: As the heat input to the heater is increased exponentially, its surface temperature also increases. Due to an increase in surface temperature, unflooded cavities with entrapped air get activated, leading to nucleation from those cavities. Upon further increase in wall temperature due to an increase in heat input, even more unflooded cavities are activated, leading to stronger bubble nucleation. Eventually at one level of wall temperature, even the cavities that are originally flooded with fluid get activated due to bubbles originating from neighboring cavities. At this point, due to the activation of a very large number of cavities, the heater wall temperature starts to decrease and the number of activated cavities again decreases. Thus, the amount of nucleation sites also drops. Hence, compared to steady state experiments, the number of active cavities at a given heat flux after the inception of boiling is lower for transient tests. This phenomena leads to a lower HTC for transient tests, compared to steady boiling tests. In other words, there is a time lag associated with the activation of all nucleation sites for transient tests, compared to steady heat flux tests. Sakurai et al conducted investigations of the mechanism to film boiling during exponentially increasing heat inputs on a solid surface, for liquid nitrogen, water and ethanol [30, 31]. For liquid nitrogen and ethanol (completely wetting fluids), they observed that a direct transition to film boiling happened from the non-boiling regime, independent of the exponential period. They suggested a new mechanism responsible for the direct transition to film boiling, and backed it by conducting photographic investigations of the solid/fluid interface. This was called Heterogeneous Spontaneous Nucleation (HSN). HSN is an explosive-process, where nucleation occurs from all cavities (flooded or unflooded) at a particular rate of increase of surface superheat. The surface temperature and the rate of increase of surface superheat, where HSN occurs, depend on the time constant of the transient. The faster the transient, the higher the HSN superheat required. Once initiated, HSN proceeds very rapidly and results in complete evaporation of the liquid in contact with the surface, thus covering the entire heater surface with a vapor film.

All the experimental efforts on nanofluids CHF to date were done for steady state conditions, i.e. the heat flux in experiments was increased in small incremental steps and was held constant at each step for a certain amount of time to allow for the achievement of a steady state. The duration of ‘steady state’ experiments typically is from several minutes to several hours. Thus, in these experiments, the nanoparticles have ample time to deposit on the surface and affect boiling behavior and hence the CHF. However, during certain reactivity-initiated accident scenarios in nuclear reactors, such as the rod ejection event, a very rapid power excursion in the fuel can occur, as fast as 0.25 – 0.50 s [35, 36]. Therefore, if nanofluids are to be used as coolants in nuclear reactors, it is important to study their CHF performance during rapid transient conditions.

3. Preparation and characterization of nanofluids

Zinc oxide (ZnO) nanoparticles dispersed in deionized water were used in the experiments. This material was chosen because Zinc is already used in nuclear reactor water coolant, as a means to reduce corrosion. Previous experiments with ZnO nanoparticles in water at MIT showed that CHF enhancement is obtained in the range of concentrations 0.001-0.1 v% [7, 37], the magnitude of the enhancement being essentially independent of nanoparticle concentration. Hence, an intermediate concentration of 0.01 v% was selected for the tests described in this paper. The

nanofluids at this target concentration were obtained by dilution with DI water of a high-concentration (30% weight) nanofluid solution provided by Nyacol Nano Technologies. The as-received nanofluids (called Nyacol DP5370 nanofluids from this point onwards), had particles of average diameters between 38 and 68 nm, as measured by Dynamic Light Scattering (DLS) which is consistent with the vendor specified size of 50 – 90 nm. The (room temperature) pH of the Nyacol DP5370 nanofluids was measured to be 8.66, which is in the right range (pH=8-10) for colloidal stability of ZnO nanoparticles in water [38]. The density of the diluted nanofluids was found to be to be 0.9985 g/cc, only slightly different from the value of pure water (0.998 g/cc), as expected, given the low nanoparticle concentration. The surface tension of the diluted nanofluids was measured, at room temperature, using the KSV Sigma 703 Digital Tensiometer, which uses the Wilhelmy Plate Method, and found to be about 71 mN/m, essentially identical to that of pure water. The thermal conductivity of the diluted nanofluids was measured at room temperature, using the KD2-pro thermal properties analyzer, and found to be the same of pure water, within the experimental uncertainty [39]. Dynamic viscosity measurements for the diluted nanofluids were carried out using a Cannon-Fenske Opaque (Reverse Flow) Viscometer, at room temperature, and again found to be identical to the viscosity of pure water. In summary, all the thermophysical properties of test nanofluids were very similar to those of pure water.

4. Experiment

The CHF was measured in the Pool Boiling Facility (PBF) shown in Figure 1. The PBF consisted of a sample/heater submerged vertically in the test fluid inside a cylindrical quartz test vessel. The transparency of quartz allowed for easy visualizations of the boiling process during the experiments. The heater was comprised of a flat SS316 sheet of 0.914 mm thickness, 34 mm length and 5 mm width. The heater was sandblasted, prior to running the experiment, in order to change its surface roughness (R_a) to 1 μm, and thus promote the formation of microcavities which can serve as bubble nucleation sites. The heater was heated resistively via two copper electrodes connected to a Genesys DC power supply capable of delivering 500 A and 20 V. During the experiments, boiling occurred on both faces of the heater, as well as along its thin lateral side. In order to verify uniformity of bath temperature in the entire test-fluid volume, two T-type thermocouples were used (one each near each end of the heater). All experiments were conducted at atmospheric pressure and saturation temperature conditions (bulk fluid temperature of 100 ^{0}C). To maintain the temperature of the test fluid, the quartz bath with its contents was placed on a hot plate. Any steam formed during the experiments was condensed back to the test pool by means of a reflux condenser which was supplied chilled water through a Lauda Chiller.

The test procedure involved loading the heater in the PBF, followed by placing the test vessel on the hot plate. The test fluid (4500 ml in volume) was then pre-heated in a 1200 W microwave oven for 40 minutes. This pre-heating would bring the test fluid temperature to roughly 85 ^{0}C. The test fluid was then transferred to the test vessel in the PBF, and further heated by the hot plate. The setup was then kept as such for 30 minutes to allow for any non-condensable gases to escape from the test fluid, and to raise the test fluid temperature to 100 ^{0}C. At this point, the initial resistance of the heater, denoted by R_{100}, was measured by passing a 3 A current through it and measuring the associated voltage drop. This value of current corresponds to a negligible heat

flux of 0.1 kW/m^2, which is small enough not to affect the heater temperature and resistance measurement. Then the experiment was conducted (as detailed below) and heat flux in the heater increased from zero until CHF occurred, which would result in heater failure and thus concluded the experiment. During the progression of each experiment, the instantaneous current passing through the heater (I) and the associated potential drop across the heated length (ΔV) were measured concurrently, which were then used to calculate the instantaneous heater resistance (R(t)). The instantaneous bulk heater temperature denoted by $T_{bulk}(t)$ was then obtained from the relation

$$T_{bulk}(t) = \frac{1}{\alpha}\frac{R(t)-R_{100}}{R_{100}} + 100 \qquad \text{Eq. 1}$$

where α is the temperature coefficient of resistivity (TCR) for SS316, measured to be 0.00117/^{0}C for our heaters in separate experiments.

4.1 Steady- state test procedure

Before running the transient CHF experiments, several experiments were conducted in steady state. The steady state CHF of DI water was used as the base case CHF. Steady state CHF was also measured for the nanofluids, to provide a relative comparison with transient CHF enhancement. For the steady state tests, after measuring R_{100}, current (I) was increased slowly, in small discrete steps, with the current kept constant at each step for 150 s to allow for the heat transfer process to reach steady state. This incremental current increase was continued until heater resistance jumped sharply indicating the occurrence of CHF. Denoting A_{ht} as the area of heat transfer, at each step, heat flux was calculated as

$$q'' = \frac{I(\Delta V)}{A_{ht}} \qquad \text{Eq. 2}$$

Each steady state test lasted approximately 30 minutes.

4.2 Transient test procedure

For the transient CHF experiments, the instantaneous heat flux was varied in time by varying the current delivered by the power supply linearly with time, going from 0 to 450 A in t_0 seconds, with t_0 characterizing the rate of flux increase. Thus, the current through the heater varied as I = 450*t/t_0 and the power generated in the heater varied (approximately) as the square of time Three values of t_0 (time frame of linear current ramp from 0 to 450 A) were explored in this paper: t_0 = 1, 10, 100 s. Since the transient tests lasted a short amount of time, they required high data acquisition rates: for I and ΔV the acquisition rate was 1000 Hz (from start of experiment to CHF). The instantaneous heater resistance and temperature were calculated as described above. In order to smoothen the data, and reduce the noise associated with the extremely fast data measurement, the current, ΔV, resistance and bulk heater temperature calculations were averaged over fixed time periods of 1000 ms, 200 ms and 25 ms, respectively, for tests with t_o = 100, 10

and 1 s, respectively. Denoting these as $\bar{I}$, $\overline{\Delta V}$, $\bar{R}$ and $\bar{T}_{bulk}$, the averaged power generated in the heater, over that time period, was calculated as

$$\bar{q} = \bar{I}(\overline{\Delta V}) \qquad \text{Eq. 3}$$

To determine the heat flux (for that time period) transferred to the fluid, one must consider that part of the total energy dissipated by Joule effect in the heater is stored as sensible heat in the heater with the rest of it transmitted to the surrounding fluid. Using the first law of thermodynamics:

$$\dot{U} = \dot{Q} - \dot{W} \qquad \text{Eq. 4}$$

where $\dot{Q}$ is the heat transfer rate from the heater to the fluid (-$\overline{q''}$s in this case), $\dot{U}$ is the rate of change of the internal energy (sensible heat) stored in the heater ($MC_p\frac{d\bar{T}_{bulk}}{dt}$) and $\dot{W}$ is the rate of electric work delivered to the heater (-$\bar{I}(\overline{\Delta V})$). The rate of change of $\bar{T}_{bulk}$ was approximated by the finite difference $\Delta\bar{T}_{bulk}/\Delta t$, where $\Delta\bar{T}_{bulk}$ is the difference between two successive values of $\bar{T}_{bulk}$ and Δt is the time difference between these measurements. The instantaneous heat flux to the fluid was then calculated by rearranging the first law as

$$\frac{v}{A_{ht}}\left(\frac{\bar{I}(\overline{\Delta V})}{v} - \rho C_p \frac{\Delta\bar{T}_{bulk}}{\Delta t}\right) = \overline{q''} \qquad \text{Eq. 5}$$

where v is the heater volume, A_{ht} is the heat transfer area, ρ is the density, and C_p is the specific heat capacity of the heater material. During the experiment, the instant when the value of $\Delta\bar{T}_{bulk}/\Delta t$ abruptly increased was defined as the point of occurrence of CHF.

The uncertainties on the current, potential drop and area of heat transfer were calculated to be less than 0.01%, 0.01%, 2% respectively. This translated to an uncertainty of less than 2% in the estimated heat flux to the fluid.

It is noteworthy that t_o is the time frame to increase the current passing through the heater linearly from 0 to 450 A. However, during the progression of the experiment, CHF occurs at $t < t_o$. The time to CHF (from initiation of experiment) for tests with t_o = 100 s, 10 s and 1 s was ~ 41 s, 5.2 s and 0.68 s, respectively. This is also seen in Figure 2, which depicts the progression of a transient DI water experiment for each value of t_o.

5. Results

Steady state CHF tests were first conducted to obtain the reference values for DI water and nanofluid CHF. The steady state tests lasted approximately 30 min. Each steady state test was performed twice to ensure repeatability. Steady state CHF was observed to increase from 511 kW/m^2 for DI water to 1298 kW/m^2 for nanofluid (an enhancement of 160%) which is consistent

with enhancements documented in literature, as discussed in Section 2.1 above. Repeatability of the transient tests was also ensured by performing each test 3 times. The longest transient tests (corresponding to t_o = 100 s) for DI water exhibited CHF similar to steady state CHF. However, the CHF for DI water increased for the shorter transients, i.e. t_o = 10 s and t_o = 1 s. Transient experiments were also performed with the nanofluids. For t_o = 100 s, the CHF was seen to increase by ~15% compared to DI water; for t_o = 10 s and t_o = 1 s, the CHF enhancement was ~36% and a negligible 2% respectively. These results are summarized in Figure 3. Post-test Scanning Electron Microscope (SEM) analysis of heaters showed a clean surface post DI water CHF but a significant porous deposit post steady state nanofluid boiling, as seen in Figure 4. Energy Dispersive X-Ray Spectroscopy (EDX) indicated that the deposit was in fact ZnO nanoparticles. Similar SEM and EDX analyses for heaters used with nanofluids in transient tests showed deposition of nanoparticles for t_o = 100 s and 10 s, but not for t_o = 1 s. These findings are shown in Figure 5. Additionally, the surface of heaters used in transient tests with DI water (all three values of t_o) was verified to be clean post-testing.

The nanoparticle layer creates a network of interconnected porosity [40] on the heater surface and also imparts a higher hydrophilicity to the surface, as revealed by contact angle measurements for a drop of DI water on post-test heater surfaces. As shown in Figure 6, surface hydrophilicty of the heater surface was increased significantly upon formation of the nanoparticle deposition layer. Similar increase in surface hydrophilicty was demonstrated by heaters used for transients characterized by t_o = 10 s and 100 s. On the other hand, as expected due to a lack of nanoparticle deposition layer, heater used for t_o = 1 s was unaffected. These observations are summarized in

Figure **7**.

Finally, the average thickness of the nanoparticle deposit was measured using confocal microscopy. To do this, part of a test heater, after nanoparticle deposition, was wiped clean with a sharp blade. Confocal scans were then obtained on an area (256 x 256 μm^2), which included the sharp transition between wiped and nanoparticle deposition areas. From the confocal data collected, the average Z-height of the areas with and without nanoparticle depositions was obtained. The difference between these heights gave the average nanoparticle deposition thickness. The results are shown in Table 1, and show that the nanoparticle deposition thickness for transients was much smaller than that of the steady state tests. However, the thickness increased with increasing transient duration.

Furthermore, to confirm that the nanoparticle deposition on the surface is indeed the cause of the CHF enhancement, experiments were also performed with heaters pre-coated with nanoparticles. Pre-coating was achieved by boiling the heaters in ZnO nanofluid for 60 minutes at 250 kW/m^2. The pre-coated heaters were then tested under transient conditions in DI water. The results were as follows: CHF enhancement with respect to the clean surface heaters was observed for all tests,

i.e. for t_o = 100/10/1 s, CHF enhancement was 36/ 46/33%, respectively. Repeating the same transient experiments with ZnO nanofluid, CHF enhancement for nanocoated heaters was 50/50/31%. These results are shown in Figure 8. Since the results for pre-coated heaters in DI water and pre-coated heaters in nanofluid are essentially identical (within experimental uncertainty), it can be concluded that the CHF enhancement comes from the nanoparticles pre-deposited on the heater surface, not the nanoparticles in the nanofluids.

6. Discussion

CHF for DI water was seen to increase from 511±10 kW/m^2 (steady-state), to 548±12 kW/m2 (t_o = 100 s), to 806±15 (t_o = 10 s) and 1497±30 kW/m^2 (t_o = 1 s). This trend is in qualitative agreement with the trends for exponential power transients reported in literature [30-33]. However, a direct quantitative comparison with those studies was not possible because of the differences in heat input ramp-up (quadratic vs exponential) and heater design (geometry and materials). The nanofluid tests led to CHF enhancement for t_o = 100 and 10 s, but not for t_o = 1 s, suggesting that the shortest transient was too fast for the nanoparticles to deposit and affect CHF. Post-test SEM imaging confirmed that ZnO nanoparticles deposit on the heater for transient tests as short as 10 and 100 s, but not 1 s. The thickness of nanoparticle deposition layers for the t_o = 100 and 10 s transients was ~0.05 μm, much smaller than that for the steady state tests (0.5-1 μm), however enough to affect CHF. Note that the maximum enhancement was obtained in the steady-state tests, which would suggest a dependence of the CHF enhancement on the coating thickness. As found in a recent study of separate surface effects on CHF [40], CHF enhancement can be achieved if a network of interconnected hydrophilic pores exists on the surface. Then the differences seen among the tests with confirmed nanoparticle deposition (i.e. steady-state, t_o = 100 and t_o = 10 s) could come from the differences in thickness, microstructure and porosity of the nanoparticle deposition layer, although this hypothesis cannot be confirmed at the present time. Finally, upon pre-coating the heater at 250 kW/m^2 for 1 hour, the CHF for DI water was increased 36, 45 and 33 % for transients with time period of 100, 10 and 1 s, respectively. Using nanofluids gave a similar enhancement. Thus, it is evident that the nanoparticle deposition layer is the cause of the CHF enhancement.

7. Conclusions

The main conclusions of this paper are as follows:

- Diluted ZnO nanofluids exhibit significant CHF enhancement compared to water for steady state pool boiling experiments on metallic plate heaters. During boiling, a porous and hydrophilic layer of nanoparticles deposits on the heater surface.
- For DI water, transient CHF is higher than steady state CHF, with CHF increasing with a decreasing duration of the transient/increasing heat flux ramp rate.
- The use of nanofluids results in CHF enhancement during the two longer transients (t_o = 10 s and 100 s), although the magnitude of enhancement is lower than steady state enhancement. Nanofluids have no effect on CHF for the fastest transient (t_o = 1 s). This indicates that a porous nanoparticle deposition layer develops in time frames as low as 10 s, but not 1 s.

- Upon pre-coating the heaters with nanoparticles, CHF enhancement is observed for all transients, confirming that CHF enhancement indeed occurs because of the nanoparticles deposited at the surface, and not the nanoparticles suspended in the nanofluid.

While this paper reports on the first experimental investigation of transient CHF in nanofluids, and in doing so it establishes the time frames required for effective nanoparticle layer deposition and CHF enhancement, questions remain about the exact mechanisms of nanoparticle deposition on the surface and its effect on CHF enhancement, at both steady and transient conditions.

Acknowledgements

This work was funded by AREVA NP; their sponsorship and support are gratefully acknowledged. The authors are also grateful to Prof. Kripa Varanasi of MIT for his valuable review of the work, and Dr. Ramakrishnan of the Schlumberger Doll Research Center for use of the confocal microscope.

References

1. U. S. Choi, Enhancing thermal conductivity of fluids with nanoparticles, in: D. A. Siginer, H. P. Wang, Development and applications of non-Newtonian glows, FED-vol. 231/MD-vol. 66, ASME, New York , 1995, pp. 99 – 105.
2. S. K. Das, S. U. S. Choi, H. E. Patel, Heat transfer in nanofluids – a review, Heat Transfer Engineering 27 (2006) 3 – 19.
3. W. M. Rohsenow, J. P. Harnett and Y. I. Cho, Handbook of Heat Transfer, third ed., McGraw-Hill, 1998.
4. S. H. Chang, W. P. Baek, Understanding, predicting and enhancing critical heat flux, The 10th International Topical Meeting on Nuclear Reactor Thermal Hydraulics, Seoul, Korea, October 5 – 9, 2003.
5. S. M. You, J. H. Kim and K. H. Kim, Effect of nanoparticles on critical heat flux of water in pool boiling heat transfer, Applied Physics Letters 83 (2003) 3374 – 3376.
6. P. Vassallo, R. Kumar and S. D'Amico, Pool boiling heat transfer experiments in silica-water nano-fluids, Int. J. Heat and Mass Tr. 47 (2004) 407 – 411.
7. S. J. Kim, I. C. Bang, J. Buongiorno, L. W. Hu, Surface wettability change during pool boiling of nanofluids and its effect on critical heat flux, Int. J. Heat Mass Tr. 50 (2007) 4105 – 4116.
8. S. M. Kwark, R. Kumar, G. Moreno, J. Yoo and S. M. You, Pool boiling characteristics of low concentration nanofluids, Int. J. Heat Mass Tr. 53 (2010) 972 – 981
9. J. S. Coursey and J. Kim, Nanofluid boiling: the effect of surface wettability, Int. J. Heat Mass Tr. 29 (2008) 1577 – 1585.
10. J. H. Kim, K. H. Kim and M. S. You, Pool boiling heat transfer in saturated nanofluids, in: Proceedings of ASME International Mechanical Engineering Congress and Exposition, Anaheim, California, 2004.

11. G. Moreno Jr., S. J. Oldenburg and S. M. You, Pool boiling heat transfer of alumina-water, zinc oxide-water and alumina-water ethylene glycol nanofluids, in: Proceedings of ASME Summer Heat Transfer Conference, San Francisco, California, 2005.
12. B. H. Truong, Determination of pool boiling critical heat flux enhancement in nanofluids, in: Proceedings of the ASME International Mechanical Engineering Congress and Exposition 8, 2007, pp. 289 – 299.
13. Z. H. Liu, X. F. Yang and J. G. Xiong, Boiling characteristics of carbon nanotube suspensions under sub-atmospheric pressures, Int. J. Thermal Sc. 49 (2010) 1156 – 1164.
14. R. Kathiravan, R. Kumar and A. Gupta, Preparation and pool boiling characteristics of copper nanofluids over a flat plate heater, Int. J. Heat Mass Tr. 53 (2010) 1673 – 1681.
15. D. Milanova and R. Kumar, Role of ions in pool boiling heat transfer of pure and silica nanofluids, Applied Physical Letters 87 (2005) 233107.
16. H. Kim, J. Kim and M. Kim, Experimental study on CHF characteristics of TiO_2-water nanofluids, Nuclear Engineering and Technology 38 (2006) 61 – 68.
17. Y. H. Jeong, W. J. Chang and S. H. Chang, Wettability of heated surfaces under pool boiling using surfactant solutions and nanofluids, Int. J. Heat Mass Tr. 51 (2008) 3025 – 3031.
18. H. Kim, H. S. Ahn and M. H. Kim, On the mechanism of pool boiling critical heat flux enhancements in nanofluids, Journal of Heat Transfer-Transactions of ASME 132 (2010) 061501.
19. D. Wen, Y. Ding, Experimental investigation into the pool bloiling heat transfer of aqueous based γ-alumina nanofluids, Journal of Nanoparticle Research 7 (2005) 265 – 274
20. S. Soltani, S. G. Etemad and J. Thibault, Pool boiling heat transfer of non-Newtonian nanofluids, Int. Comm. Heat Mass Tr. 37 (2010) 29 – 33.
21. A. Suriyawong and S. Wongwises, Nucleate pool boiling heat transfer characteristics of TiO_2-water nanofluids at very low concentraions, Exp. Thermal Fluid Sc. 34 (2010) 992 – 999.
22. I. C. Bang and S. H. Chang, Boiling heat transfer performance and phenomena of Al_2O_3-water nano-fluids from a plain surface in a pool, Int, J. Heat and Mass Tr 48 (2005) 2407 – 2419.
23. S. K. Das, N. Putra and W. Roetzel, Pool boiling characterisitcs of nano-fluids, Int. J. Heat and Mass Tr. 46 (2003) 851 – 862.
24. S. K. Das, N. Putra and W. Roetzel, Pool boiling of nano-fluids on horizontal narrow tubes, Int. J. Multiphase Flow 29 (2003) 1237 – 1247.
25. H. A. Johnson, Transient boiling heat transfer, Int. J. Heat Mass Tr. 14 (1971) 67 – 82
26. A. Sakurai and M. Shiotsu, Temperature-controlled pool boiling heat transfer, Heat Transfer IV (1974) B3.1.
27. A. Sakurai and M. Shiotsu, Transient pool boiling heat transfer. Part I: Incipient boiling superheat, J. Heat Tr. 99 (1977) 547 – 553.
28. A. Sakurai, K. Mizukami and M. Shiotsu, Experimental studies on transient boiling heat transfer and burnout, Heat Transfer V (1970) B3.4.
29. A. Sakurai and M. Shiotsu, Transient pool boiling heat transfer. Part II: Boiling heat transfer and burnout, J. Heat Tr. 99 (1977) 554 – 560.
30. A. Sakurai, M. Shiotsu and K. Hata, New transition phenomena to film boiling due to increasing heat inputs on a solid surface in a pressurized liquid, HTD-Vol. 260/FED-Vol. 169. Instability in Two-Phase Flow Systems, ASME Annual Winter Meeting New Orleans (1993) 27 – 39.

31. A. Sakurai, Mechanisms of transitions to film boiling at CHFs in subcooled and pressurized liquids due to steady and increasing heat inputs, Nuclear Engineering and Design 197 (2000) 301 – 356 .
32. A. Sakurai, M. Shiotsu, K. Hata and K. Fukuda, Transition phenomena from non-boiling regime to film boiling on a cylinder surface in highly subcooled and pressurized water due to increasing heat inputs, ASME Paper 95-WA/HT-17 (1995) 1 – 11.
33. J. Park, K. Fukuda and Q. Liu, Effects of surface conditions on transient pool boiling CHF in various liquids with different mechanisms depending on pressure and subcooling, JSME Int. Journal Series B 49 (2) (2006) 318 – 325.
34. V. Carey, Liquid-Vapor Phase-Change Phenomena, Second Ed. Taylor & Francis, 2008.
35. M. Hursin and T. Downar, PWR control rod ejection analysis with the MOC code decart, in: Joint International Workshop: Nuclear Technology and Society – Needs for Next Generation, Berkeley, California, January 6 – 8, 2008.
36. H. Finnemann, H. Bauer, A. Galati and R. Martinelli, Results of LWR core transient benchmarks, NEA/NSC/DOC(93) 25, October 1993.
37. S. J. Kim, I. C. Bang, J. Buongiorno, L. W. Hu, Surface wettability change during pool boiling of nanofluids and its effect on critical heat flux, Int. J. Heat Mass Tr. 50 (2007) 4105 – 4116.
38. Personal e-mail communication with AREVA NP, Technical Center, Chemical Department, Le Creusot, France, May 4, 2010.
39. J. Buongiorno, D. C. Venerus, N. Prabhat, T. McKrell, J. Townsend, R.Christianson, Y. V. Tolmachev, P. Keblinski, L.W. Hu, J. L. Alvarado, I.C. Bang, S. W. Bishnoi, M. Bonetti, F Botz, A. Cecere, Y. Chang, G. Chen, H. Chen, S. J. Chung, M. K. Chyu, S. K. Das, R. Di Paola, Y. Ding, F. Dubois, G. Dzido, J. Eapen, W. Escher, D. Funfschilling, Q. Galand, J. Gao, P. E. Gharagozloo, K. E. Goodson, J. G. Gutierrez, H. Hong, M. Horton, K. S. Hwang, C. S. Iorio, S. P. Jang, A. B. Jarzebski, Y. Jiang, L. Jin, S. Kabelac, A. Kamath, M. A. Kedzierski, L.G. Kieng, C. Kim, J. H. Kim, S. Kim, S. H. Lee, K. C. Leong, I. Manna, B. Michel, R. Ni, H. E. Patel, J. Philip, D. Poulikakos, C. Reynaud, R. Savino, P. K. Singh, P. Song, T. Sundararajan, E. Timofeeva, T. Tritcak, A. N. Turanov, S.V. Vaerenbergh, D. Wen, S. Witharana, C. Yang, W. H. Yeh, X-Z. Zhao, and S-Q. Zhou, A Benchmark Study on the Thermal Conductivity of Nanofluids, J. Applied Physics, 106, 2009, 094312.
40. H. O'Hanley, "Separate effects of surface roughness, wettability and porosity on boiling heat transfer and critical heat flux and optimizing of boiling surfaces", SM Thesis, Massachusetts Institute of Technology, Cambridge, MA, 2012.

Figure Captions

Figure 1: Schematic of PBF used for experiments (front view).

Figure 2: Progression of heat flux during transient DI water experiment for each value of t_o. The curves terminate at CHF for each experiment.

Figure 3: Test results for various transient tests, both for DI water and nanofluid. Also shown are the DI water and nanofluid CHF obtained for steady state tests. The error bars show the standard deviation in measured CHF data.

Figure 4: Post-test SEM images for heaters used in steady state experiments showing a clean surface for heaters used with DI Water (a) and deposit made of nanoparticles on heaters boiled in nanofluid (b).

Figure 5: Post-test SEM images for heaters used in transient experiments with nanofluids showing nanoparticle deposition for t_o = 100 s (a), 10 s (b) and a clean surface for t_o = 1 s (c).

Figure 6: Static contact angle measurement for DI water on unused heater (a) and heater boiled in nanofluid for a steady state test (b). The increased hydrophilicty due to nanoparticle deposition layer is demonstrated by the drastic decrease in contact angle of water.

Figure 7: Static contact angle measurement for DI water on heater tested in nanofluid for (a) t_o = 1 s, (b) t_o = 10 s and (c) t_o = 100 s. The heater surface for the shortest transient appears to be unchanged, in terms of surface hydrophilicity, while the hydrophilicity of heaters from the other two transients is markedly increased.

Figure 8: Transient test results for bare and pre-coated heaters in both DI water and nanofluid. The error bars plot the standard deviation in the measured CHF data.

Tables

Table 1: Summary of nanoparticle deposition thickness measurements

Nanofluid Experiment Description	Average Nanoparticle Deposition Thickness (μm)
Steady State	0.76
t_o = 100 s	0.06
t_o = 10 s	0.04
t_o = 1 s	N/A

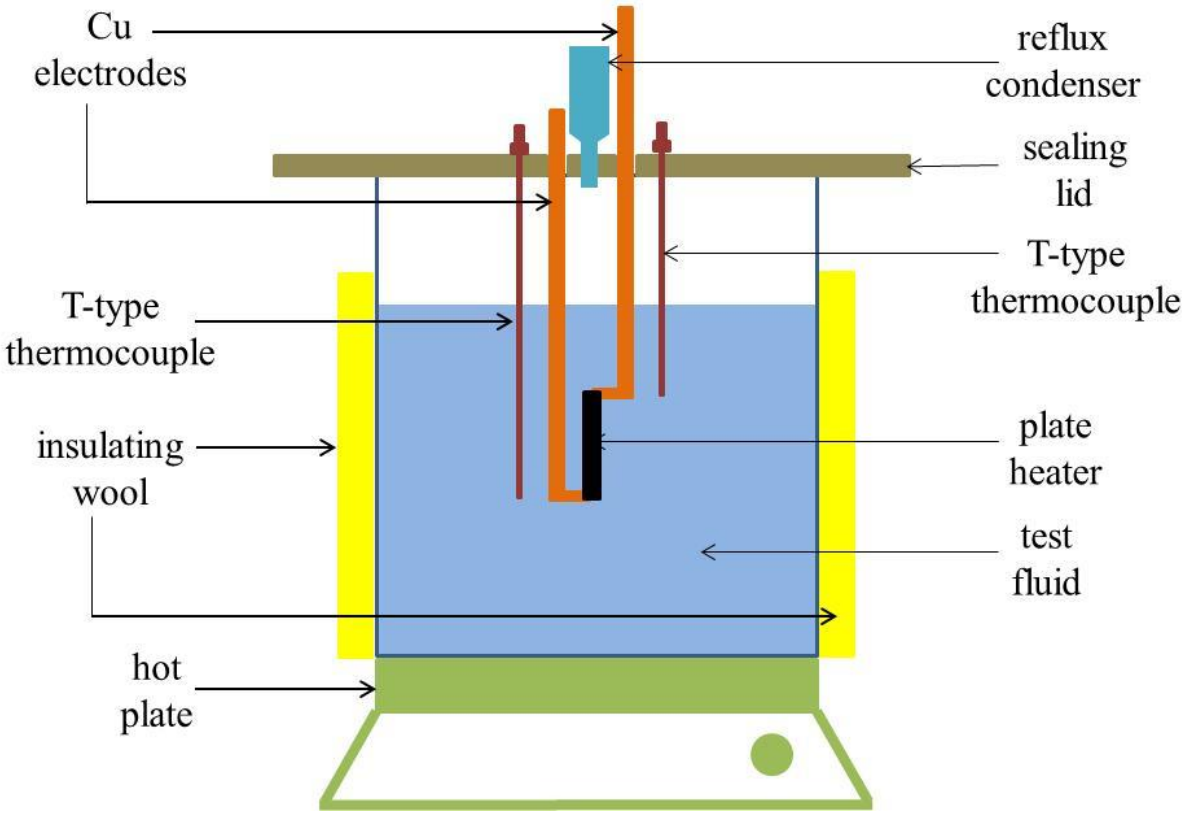

Figure 9: Schematic of PBF used for experiments (front view).

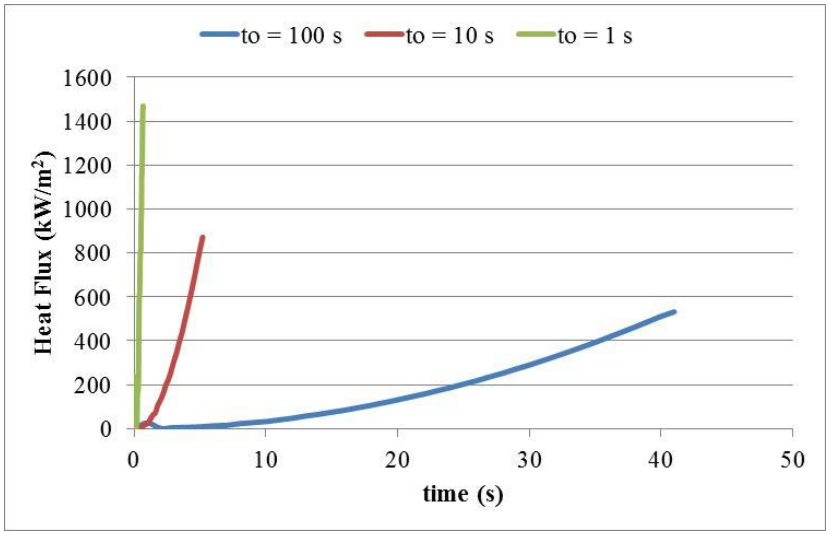

Figure 10: Progression of heat flux during transient DI water experiment for each value of t_o. The curves terminate at CHF for each experiment.

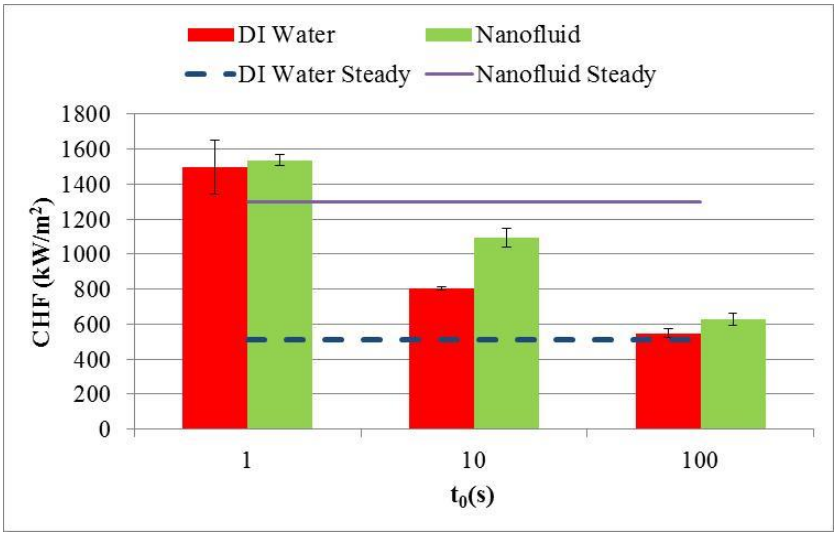

Figure 11: Test results for various transient tests, both for DI water and nanofluid. Also shown are the DI water and nanofluid CHF obtained for steady state tests. The error bars show the standard deviation in measured CHF data.

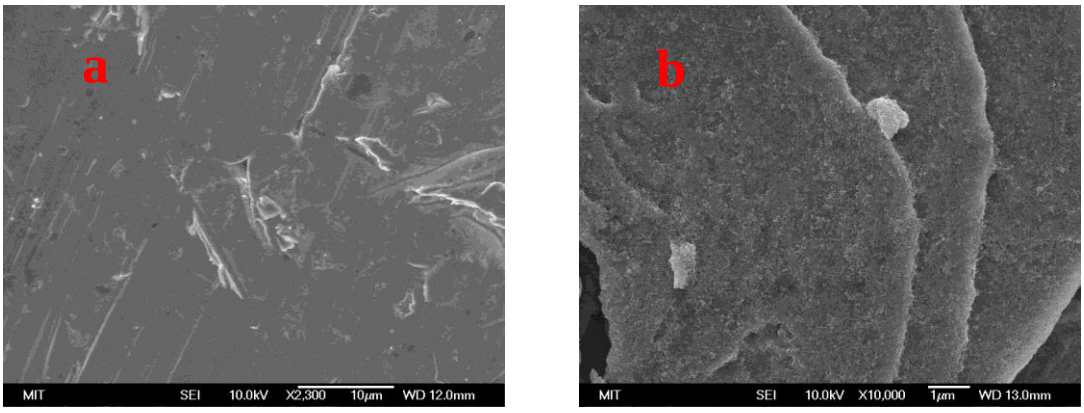

Figure 12: Post-test SEM images for heaters used in steady state experiments showing a clean surface for heaters used with DI Water (a) and deposit made of nanoparticles on heaters boiled in nanofluid (b).

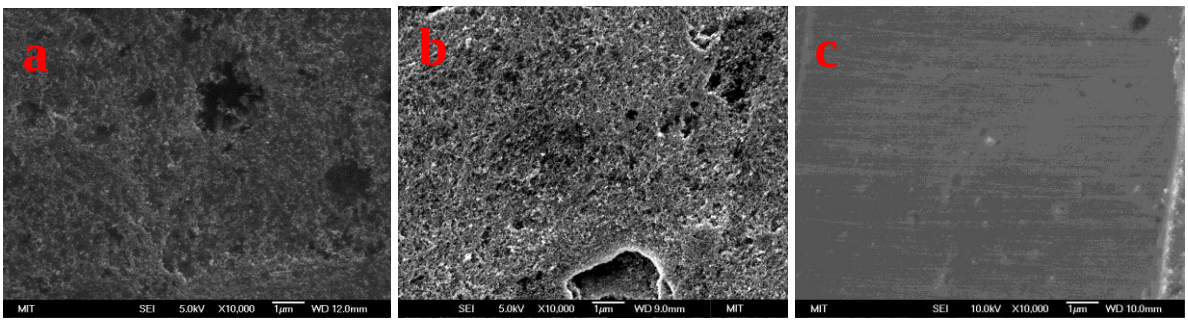

Figure 13: Post-test SEM images for heaters used in transient experiments with nanofluids showing nanoparticle deposition for t_o = 100 s (a), 10 s (b) and a clean surface for t_o = 1 s (c).

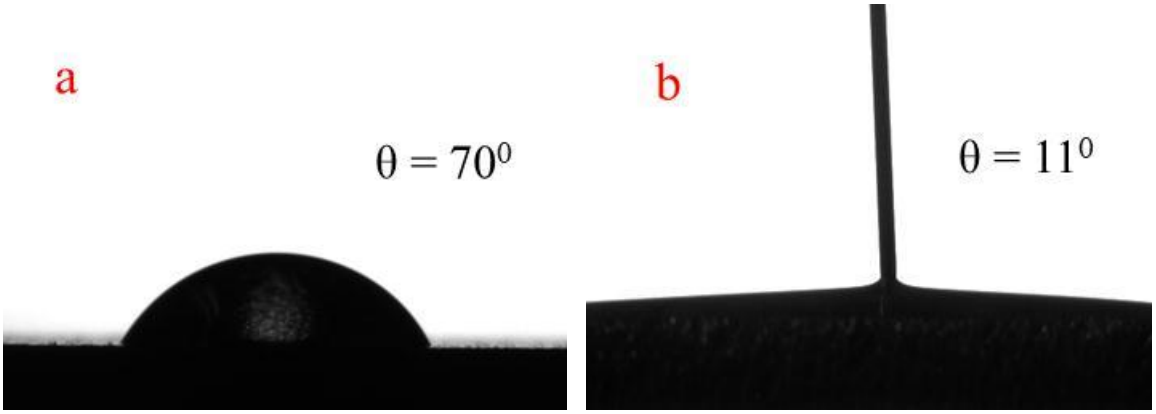

Figure 14: Static contact angle measurement for DI water on unused heater (a) and heater boiled in nanofluid for a steady state test (b). The increased hydrophilicty due to nanoparticle deposition layer is demonstrated by the drastic decrease in contact angle of water.

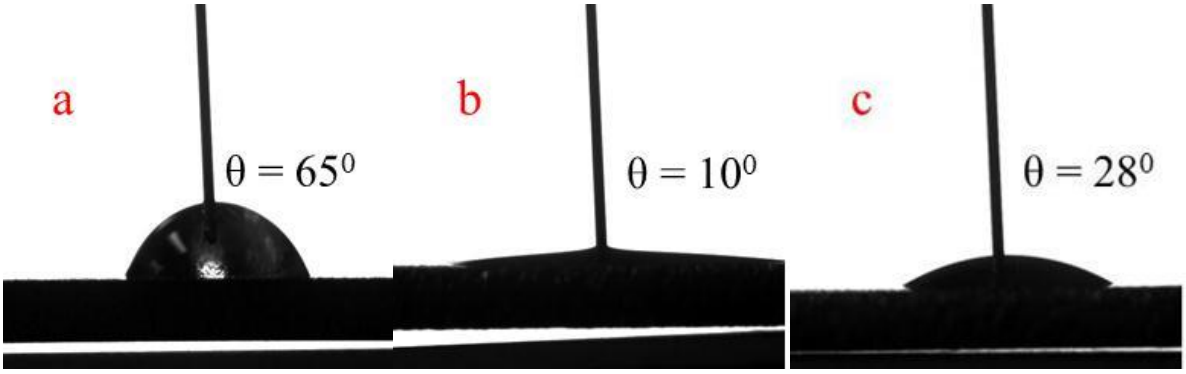

Figure 15: Static contact angle measurement for DI water on heater tested in nanofluid for (a) t_o = 1 s, (b) t_o = 10 s and (c) t_o = 100 s. The heater surface for the shortest transient appears to be unchanged, in terms of surface hydrophilicity, while the hydrophilicity of heaters from the other two transients is markedly increased.

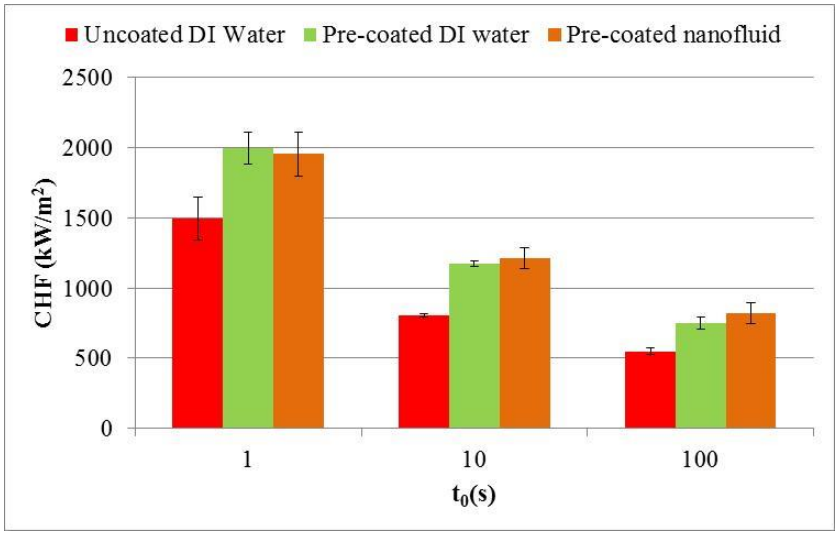

Figure 16: Transient test results for bare and pre-coated heaters in both DI water and nanofluid. The error bars plot the standard deviation in the measured CHF data.